Sensors and Actuators B 166–167 (2012) 141–149

Contents lists available at SciVerse ScienceDirect

Sensors and Actuators B: Chemical

journal homepage: www.elsevier.com/locate/snb

Impact of Nb doping on gas-sensing performance of TiO_2 thick-film sensors

Wen Zeng[a,*], Tianmo Liu[a], Zhongchang Wang[b,*]

[a] College of Materials Science and Engineering, Chongqing University, Chongqing 400030, PR China
[b] WPI Research Center, Advanced Institute for Materials Research, Tohoku University, 2-1-1 Katahira, Aoba-ku, Sendai 980-8577, Japan

ARTICLE INFO

Article history:
Received 11 September 2011
Received in revised form 8 February 2012
Accepted 9 February 2012
Available online 3 April 2012

Keywords:
TiO_2
Nb doping
Volatile organic compounds
Oxygen adsorption

ABSTRACT

Using a simple hydrothermal method, the pristine and Nb doped TiO_2 is prepared, and their microstructures and gas-sensing responses to the harmful volatile organic compounds are investigated with a special focus on the impact of Nb additive. We find that the gas response of TiO_2 is enhanced significantly by doping Nb, which is understood in theory upon proposed adsorption models. Combining experimental measurements with first-principles calculations, the working mechanism underlying such improvement in gas-sensing functions by the Nb additive is discussed.

1. Introduction

The indoor air quality has become a serious environmental issue in our daily life. Indoor pollutants, which mainly consist of volatile organic compounds (VOCs) such as the formaldehyde, ethanol, xylene and acetone, are known to be one of the causes to deteriorate the health of human being or even result in terrible diseases [1–3]. To solve this problem, much effort has been devoted to the development of a reliable gas sensor that can pursue an *on-site* detection of the VOC gases in a smart fashion [4–8]. Among all the gas-sensing materials, the semiconducting metal oxides have long been recognized as being promising in monitoring the harmful VOC gases on an industrial level owing to their high response as well as low manufacture cost [9–15]. However, the widespread use of such oxides as gas-sensing materials is currently restrained by the absence of selectivity and durability, the fundamental requirements for a practical application of gas sensors [16,17].

Of all the traditional semiconducting metal oxides, TiO_2 has been demonstrated to hold a substantial promise for sensor devices largely because it is chemically stable even at high temperatures [18–20]. Further, exotic elements can often be incorporated into TiO_2 as additives, which indeed enable a dramatic improvement in its gas-sensing performances, including La, W and Nb [21–23]. Of these additives, the Nb is found to be very effective in enhancing gas responses of TiO_2 to NO_2 [24], shortening response time to O [25], and upgrading photosensitivity to NO [26]. One plausible explanation for such enhancement in gas-sensing properties of TiO_2 is that the introduction of Nb can mediate elegant shift in electronic structures of TiO_2, for instance, displacement of location of Fermi level (E_F) with respect to the conduction band of TiO_2 [27,28], and presence of novel occupied states arising from the Nb 4d valence electrons that form nonbonding bands in the bulks, whereas localized dangling bonds on the surfaces [29]. Structurally, Anukunprasert et al. has provided convincing evidence that the addition of Nb can retard the phase transformation of TiO_2 from the anatase to rutile as well as inhibit its inner grains from growing. Such structural and electronic modifications due to the Nb have a direct consequence on the gas-sensing ability of TiO_2 by enhancing its response to e.g., CO [30,31] and ethanol [31,32], whichever method is applied to fabricate such systems. In addition, previous reports have also claimed that the surface morphology of TiO_2 can be tailored efficiently by doping Nb as well, such as the pore, particle size, and specific surface area [33–35]. However, the working mechanism of TiO_2 sensors and how the Nb impacts gas-sensing behaviors of TiO_2 remain a mystery, in particular, the atomic geometry and chemical environment on the oxide surface, which strongly affect the gas-sensing performances, are hardly accessible.

Here, we have prepared the pristine and Nb doped TiO_2 nanocomposites *via* the simple yet efficient hydrothermal method and investigated their gas-sensing responses towards VOCs including methanol, ethanol, acetone and formaldehyde. To gain more insight into gas-sensing mechanism, we conduct a series of first-principles calculation based upon the surface adsorption models inferred from experiments. The Nb doped TiO_2 is found to exhibit enhanced gas response to VOCs as compared to pristine TiO_2, and our simulations

* Corresponding authors. Current address: College of Materials Science and Engineering, Chongqing University, Chongqing 400030, China. Tel.: +86 23 65102465; fax: +81 22 217 5930.
E-mail addresses: wenzeng@cqu.edu.cn (W. Zeng), zcwang@wpi-aimr.tohoku.ac.jp (Z. Wang).

0925-4005/$ – see front matter © 2012 Elsevier B.V. All rights reserved.
doi:10.1016/j.snb.2012.02.016

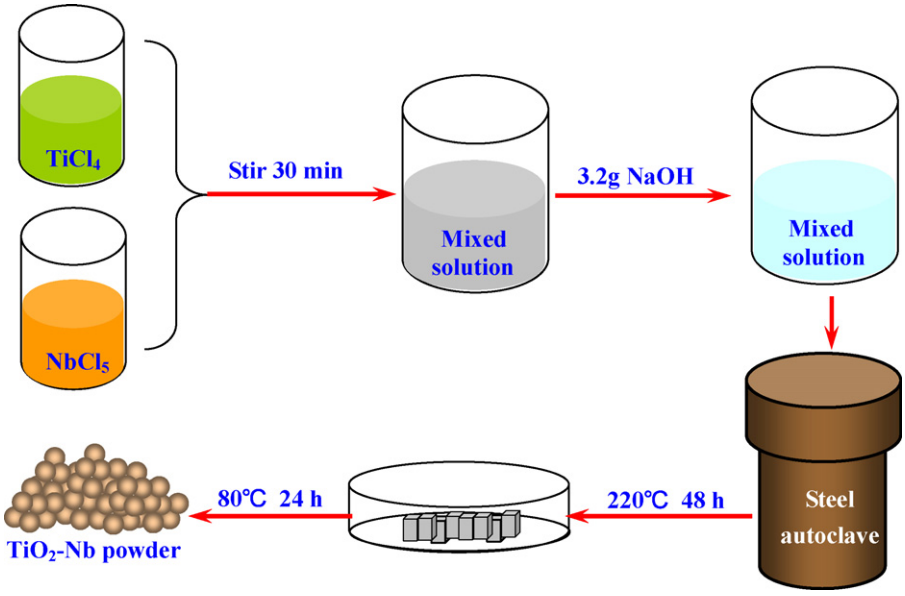

Fig. 1. Flow diagram of preparation process of Nb doped TiO_2 nano-composites.

open up a new avenue to understanding gas-sensing origin of the TiO_2-based sensing materials.

2. Experimental

2.1. Preparation of Nb-doped TiO_2 nano-composites

All chemical reagents were of analytical grade and applied without any further purification. The pristine and Nb doped TiO_2 nano-composites were fabricated using the hydrothermal method, the process of which was illustrated schematically in Fig. 1. The metal salt were first hydrolyzed in dilute ammonium hydroxide solution and then 0.02 M of $TiCl_4$ was dissolved in 50 mL of distilled water, followed by the addition of 0.16 g of $NbCl_5$ in a drop-by-drop fashion under intense magnetic stirring for 30 min. The molar mass ratio of Nb ions to the total metallic ions was fixed to 3%, taking into account the report that the Nb with concentration of 2.5–3% may significantly modify electronic and gas-sensing properties of TiO_2. Further, the NaOH (3.2 g) was slowly dropped to the mixed solution under intense stirring. The mixed solution was finally transferred into steel autoclaves (50 mL), which were sealed and maintained at 220 °C for 48 h. The white product was harvested upon pursing centrifugation, washing away the unwanted ions with ethanol for several times, and drying at 80 °C in air for 24 h. For the purpose of comparison, pristine TiO_2 was prepared by an analogous process.

2.2. Microstructural characterization

Microstructural analyses of the obtained powders were performed using X-ray diffraction (XRD), scanning electron microscopy (SEM), and transmission electron microscopy (TEM). For the XRD, the Shimadzu XD-5A diffractometry with Cu Kα radiation operated at 30 kV and 100 mA was applied. The surface morphologies were observed using the JEOL JSM-5510 SEM, and structures were characterized using the JEOL JEM-4000EX high-resolution TEM (HRTEM). The specific surface area was obtained upon the multi-point Brunauer–Emmett–Teller (BET) analyses of nitrogen adsorption isotherms recorded on the surface area analyzer.

2.3. Fabrication of gas sensors

Gas sensors were fabricated by first mixing the powders with diethanolamine and ethanol so as to form slurry suspension. To obtain thick films, this suspension was then screen printed onto an alumina tube with a pair of gold electrodes located at the both end sides of the tube (Fig. 2). The coated alumina tubes were dried at 100 °C for 2 h and subsequently calcinated at 350 °C for 1 h. The distance between two electrodes was estimated to be 6 mm and diameter of the tube 1.2 mm. Thickness of the film was ~100 μm. Next, a Ni–Cr wire was inserted into the tube, serving as a heater. Finally, the gas sensors were aged at 200 °C for 240 h to improve stability and repeatability.

2.4. Measurement of gas-sensing properties

Gas-sensing properties were measured using a static HW-30A system controlled by computer (Hanwei Electronics Co., Ltd.), as illustrated in Fig. 3. The sensors were operated by loading a circuit voltage of V_c, which allowed an output voltage of V_{out}. The operating

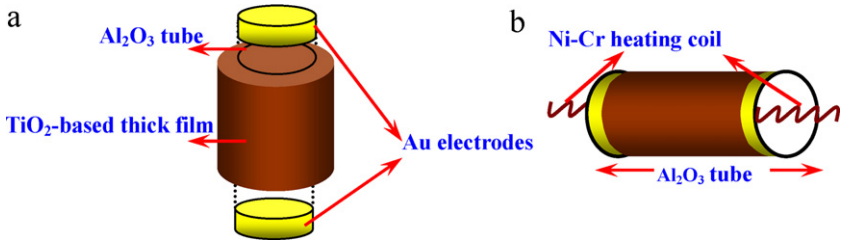

Fig. 2. Schematic outline of the fabricated gas sensor: (a) vertical and (b) horizontal view.

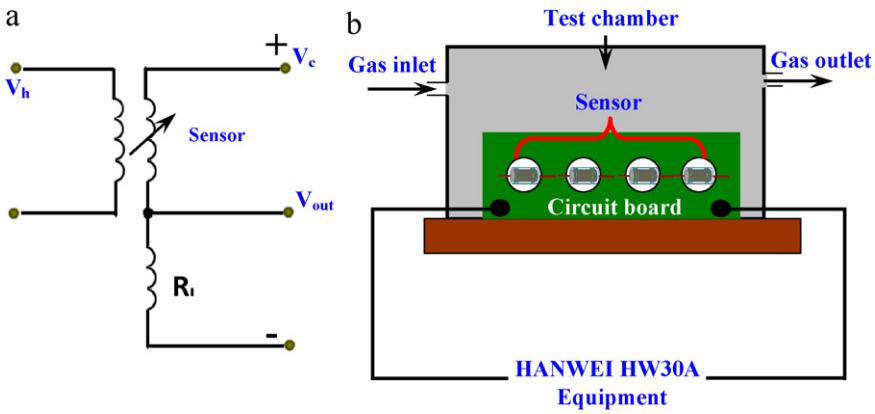

Fig. 3. (a) Scheme of electric circuit in sensor device. (b) Gas-sensing measurement system.

Table 1
The lattices parameters of undoped and Nb-doped TiO_2 unit cell.

	a (Å)	*c* (Å)
TiO_2	3.785	9.514
TiO_2–Nb	3.786	9.514

temperature of gas sensors can be adjusted by altering the current flow across the heater. Gas concentration was controlled through injecting a given amount of target gas into the glass chamber *via* a needle valve (Fig. 3(b)). The gas response (S) was calculated from the expression $S = R_a/R_g$, where R_a and R_g were resistances of the sensor in air and test gas, respectively, measured by monitoring the output voltage V_{out}. All gas-sensing experiments were conducted under laboratory conditions, i.e., at room temperature with a relative humidity of 40%.

3. Results and discussion

3.1. Structural characterization

Fig. 4 presents the XRD spectra of the pristine and Nb doped TiO_2, where the textural orientations of the detected matters are given as well for easy reference. The diffraction peaks in each sample are consistent well with those of a standard TiO_2 with anatase phase (JCPDS 21-1272), indicating that the prepared products are chemically pure. However, no diffraction peak regarding the Nb is detected in the doped samples, which is attributed to the small amount of added Nb that is beyond the detection limit, and indicates that no Nb compounds are formed. To probe whether the

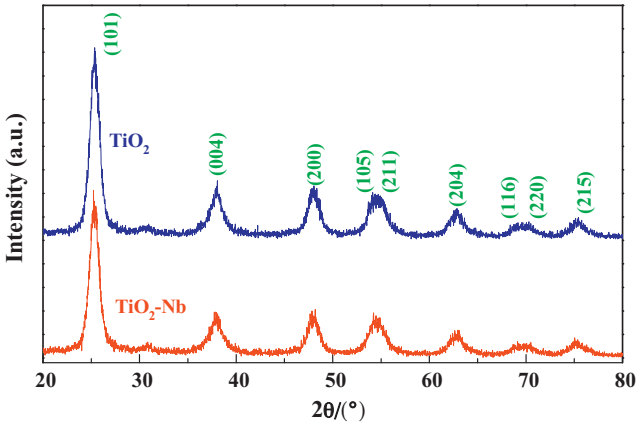

Fig. 4. X-ray diffraction patterns of the TiO_2 powders with and without Nb doping.

Table 2
EDX of the samples.

Element	TiO_2		TiO_2–Nb	
	Weight%	Atomic%	Weight%	Atomic%
O K	34.48	59.83	34.27	61.64
Ti K	65.52	40.15	62.11	37.23
Nb L			3.62	1.12

added Nb can incorporate into TiO_2 lattice, we further compute the lattice parameters upon the XRD data, as listed in Table 1, where one can see that the lattice constants undergo a minor change *via* Nb doping, indicating that Nb may partially fill the cation sites that would normally be occupied by Ti atoms owing to the similarity in ionic radius between Ti^{4+} and Nb^{5+} [36].

The SEM images of the pristine and Nb doped TiO_2 are shown in Fig. 5(a) and (b), where they both exhibit a nanoparticle feature with a uniform size and shape. A closer inspection reveals that these nanoparticles are almost in a rice-like morphology with diameter ranging from 18 nm to 30 nm, which is supported from the TEM image showing a size of 20–25 nm for the Nb doped TiO_2 (Fig. 5(c)). Fig. 5(d) presents HRTEM image of the doped sample, where one can see well developed lattice fringes, providing evidence that the prepared TiO_2 powder is of high crystallinity. Further energy-dispersive X-ray spectroscopy (EDS) analyses confirm that the pristine sample is composed of Ti and O only (Fig. 5(e)), whereas the doped one Nb, Ti and O (Fig. 5(f)), in accordance with the chemical composition of the prepared powders (Table 2). This further demonstrates that Nb is successfully incorporated into the TiO_2, although it is unable to be detected in the XRD spectra.

Table 3 presents the measurement data on the specific surface area and porosity, both of which are the key factors in affecting gas-sensing performances. The specific surface area was obtained using the BET method, and the total pore volume (V_p) and average pore diameter (d_p) were determined from the Barrett–Joyner–Halenda (BJH) desorption isotherm. The specific surface area of the Nb doped TiO_2 is estimated to be 19.5 m^2/g, somewhat larger than that of the pristine TiO_2 (18.4 m^2/g). The total pore volume and average pore diameter are evaluated to be 0.02 cm^3/g and 12 nm for the pristine TiO_2, which are almost the same as those of the doped case (0.03 cm^3/g and 12 nm). These, together with the close specific

Table 3
BET surface area and pore structure parameters for the samples.

Sample	S_{BET} (m^2/g)	V_P (cm^3/g)	d_P (nm)
TiO_2	18.4	0.02	12
Nb–TiO_2	19.5	0.03	12

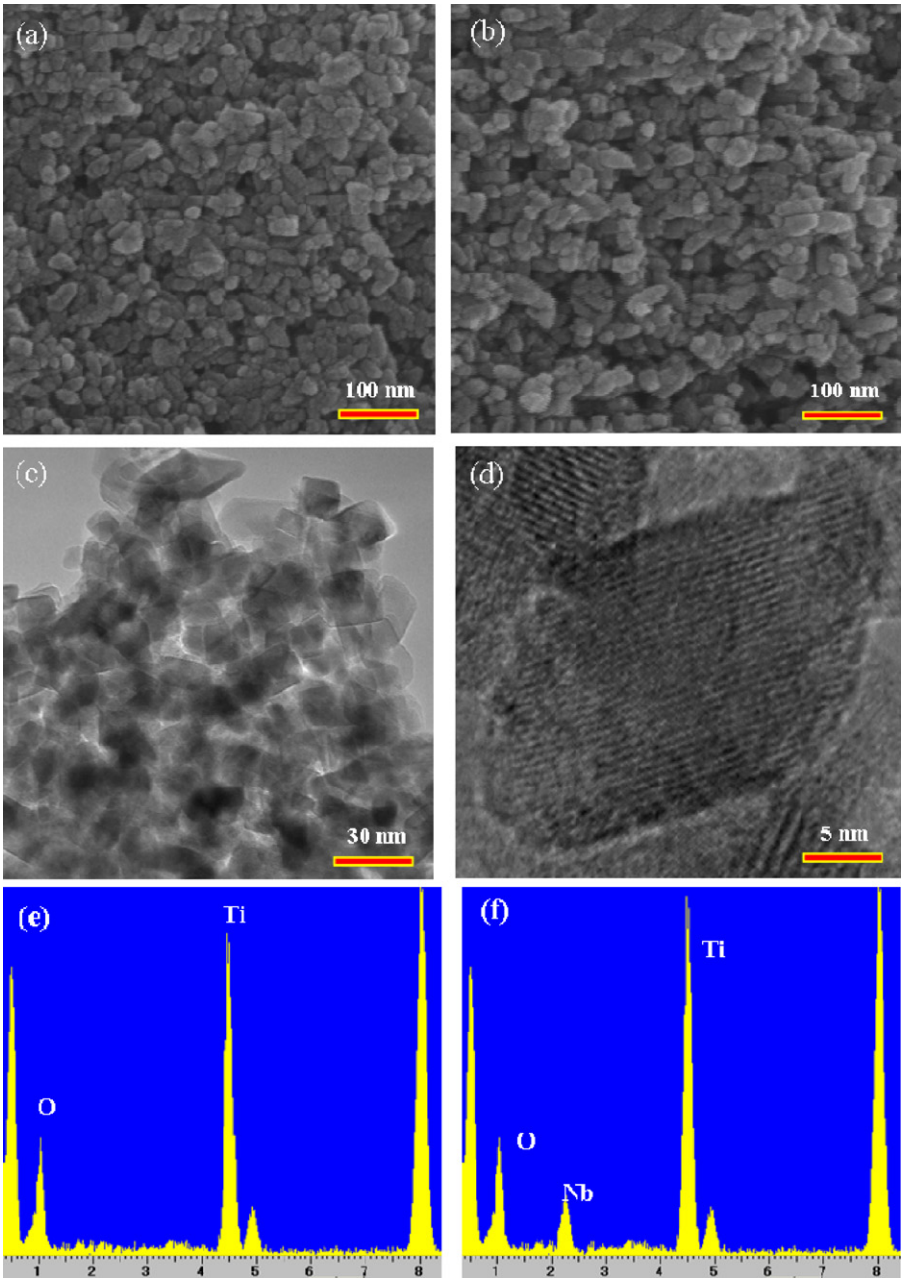

Fig. 5. SEM micrographs of (a) pristine and (b) Nb doped TiO_2. (c) TEM and (d) HRTEM image of the Nb doped TiO_2. The EDS spectra for the pristine and Nb doped TiO_2 are shown in (e) and (f), respectively.

surface area and morphology, suggest that the Nb doping imposes only minor influence on the microstructure of TiO_2.

3.2. Gas-sensing properties

To investigate how Nb affects gas-sensing properties of TiO_2, we first present in Fig. 6 gas responses of both pristine and Nb doped TiO_2 toward several VOCs such as methanol, ethanol, formaldehyde and acetone at various operating temperatures under a concentration of 500 ppm. Evidently, the sensor made of doped TiO_2 shows a higher response, lower optimum operating temperature (380–400 °C in doped case, whereas 450 °C in pristine case), and better gas-sensing performance than the sensor made of pristine TiO_2, regardless of the species of test gas, inferring that the sensing functions of TiO_2 to VOCs are improved *via* doping. Fig. 7 shows gas response of the sensors under different gas concentrations at an operating temperature of 400 °C. The response increases linearly with no sign of saturation as the concentration increases from 100 to 800 ppm, whichever gas is introduced. Again, the sensor made of doped TiO_2 show a larger response to VOCs as compared to the one made of pristine TiO_2, implying that the Nb doped TiO_2 nanocomposites are promising for developing a sensor device that can monitor the harmful VOC gases in an effective way.

Fig. 8 illustrates repetitive response and recovery characteristic for the sensors with and without Nb. The sensors are operated at 400 °C under a concentration of 500 ppm. The voltage increases in both cases when gas is in yet returns to its original state once the gas is out. The key difference between the two sensors is that the extent in increase of voltage in the doped case is pronouncedly larger than that in the clean one, which verifies again that the Nb can improve gas performances of TiO_2 and thus is an effective dopant in improving the sensing response of TiO_2 to VOCs.

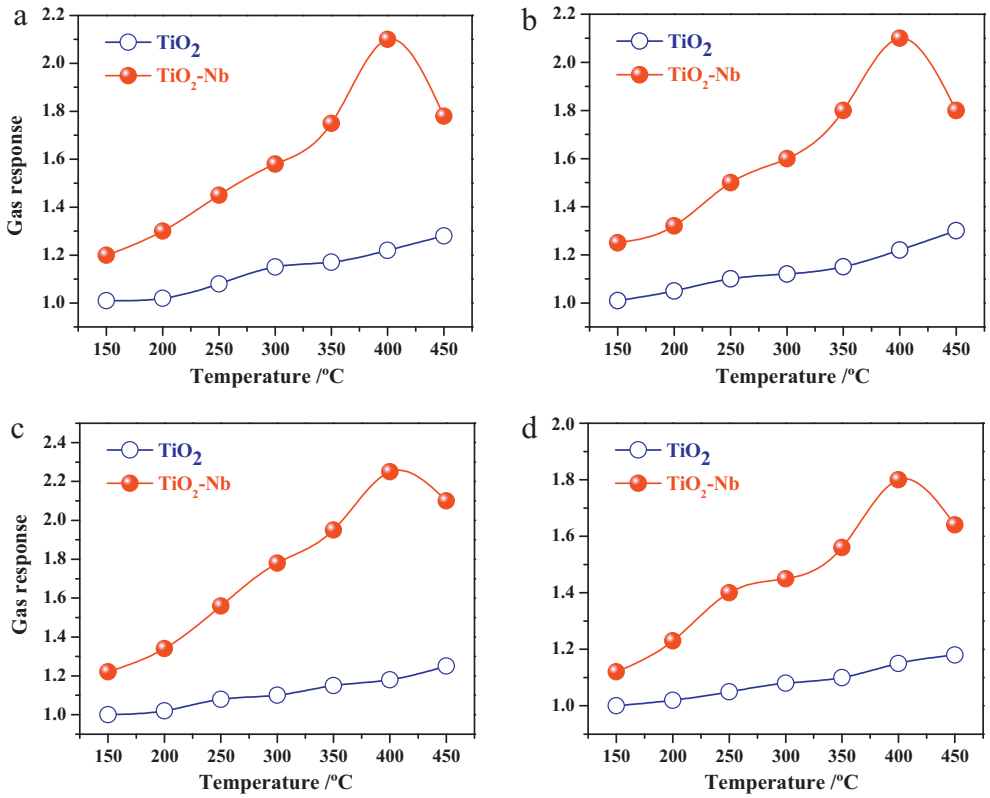

Fig. 6. Gas response of the TiO_2 sensors as a function of the operating temperature measured at (a) ethanol, (b) methanol, (c) formaldehyde and (d) acetone atmosphere.

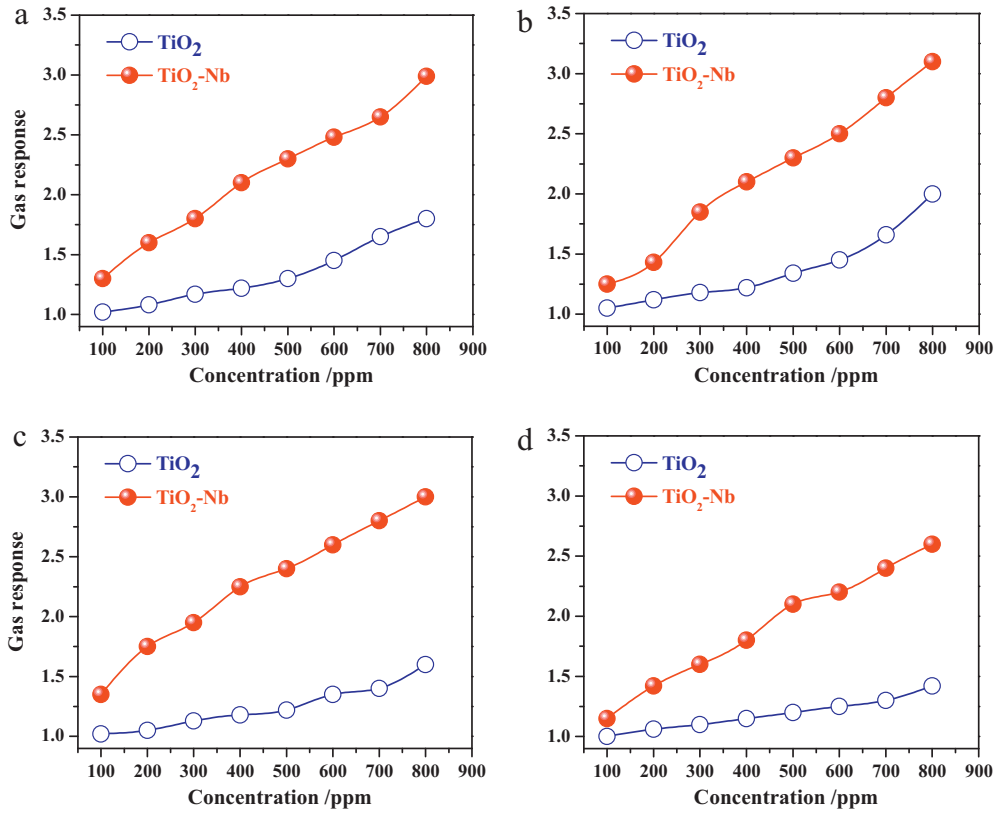

Fig. 7. Gas response of the TiO_2 sensors as a function of the gas concentration measured at (a) ethanol, (b) methanol, (c) formaldehyde and (d) acetone atmosphere.

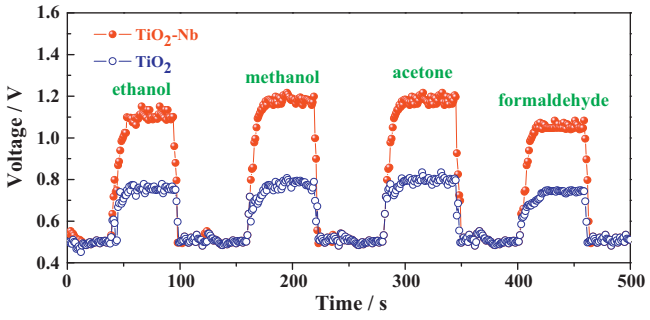

Fig. 8. Response and recovery characteristics of the TiO_2 gas sensors.

Table 4
Formation energy of Nb-doped TiO_2 (1 0 1) face.

	Dopant formation energy
Ti_{5C}	3.48 eV
Ti_{6C}	4.52 eV

3.3. Gas-sensing mechanism

The gas-sensing function of TiO_2 is known to be due to the adsorption of oxygen on surface, which extracts the valence electrons, leading to an increase in conductivity. The absorbed O can induce a depletion layer, bending the surface bands and thereby increasing the energy barrier (i.e., resistance) of the gas sensors. Once the test gas is in, chemical reaction takes place between the gas molecule and pre-adsorbed ionized oxygen, which releases electrons back onto the oxide surface, enhancing conductivity of the sensors [37,38]. To shed more light of the O adsorption process and clarify the sensing mechanism of TiO_2, we perform a first-principles study of the O reactions on a (1 0 1) surface of anatase TiO_2, taking into account the effect of Nb doping. The (1 0 1) surface has been chosen purposely because it is thermodynamically stable and widely adopted to simulate the surface of anatase TiO_2 [39–45].

The anatase TiO_2 bulk belongs to the tetragonal $D_{4h}^{19} - I4_1/amd$ space group with $a = 3.782$ Å and $c = 9.502$ Å [46]. To simulate surfaces, a vacuum region of 15 Å was embedded along the surface normal to eliminate the unwanted interaction between the slab and its period images. Fig. 9(a) shows the surface model, wherein the O fills either two-fold (O_{2C}) or three-fold (O_{3C}) coordinated sites, and the Ti fills five-fold (Ti_{5C}) or six-fold (Ti_{6C}) coordinated

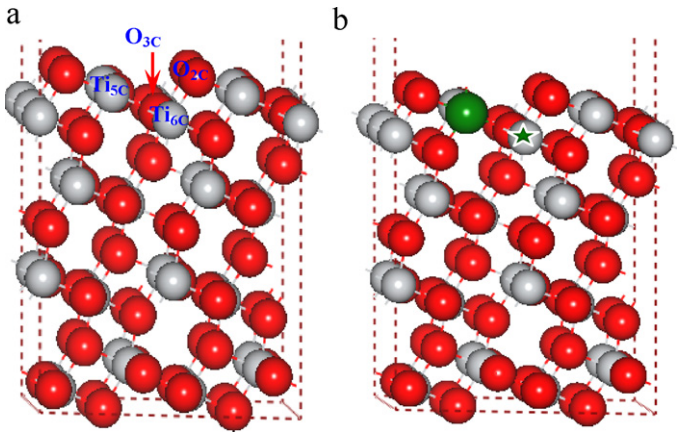

Fig. 9. Atomic geometries of (a) clean anatase TiO_2 (1 0 1) surface (b) Nb doped (1 0 1) surface. The red, gray and green balls represent O, Ti and Nb atoms, respectively. The stars in green indicate the doping positions.. (For interpretation of the references to color in this figure legend, the reader is referred to the web version of the article.)

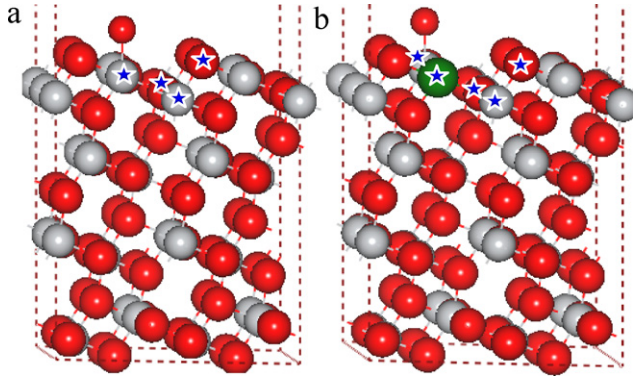

Fig. 10. Models of the oxygen adsorption on (a) clean and (b) Nb doped (1 0 1) surface of TiO_2. The stars in blue indicate the adsorption sites. (For interpretation of the references to color in this figure legend, the reader is referred to the web version of the article.)

sites. Calculations of total energy and electronic structure were conducted using the VASP code within density functional theory (DFT) [47]. The Perdew–Burke–Ernzerhof (PBE) form of generalized gradient approximation (GGA) was used to describe the exchange-correlation functional [48]. We applied the projector augmented-wave method with $6 \times 6 \times 1$ k-point grids and a cut-off energy of 360 eV, which ensure an energy convergence to within 1–2 meV/atom.

To explore the energetically stable site for Nb, we considered two likely models by substitution of Nb for individual Ti_{5C} or Ti_{6C} atom on the optimized (1 0 1) surfaces [49] (Fig. 9(b)). The impurity

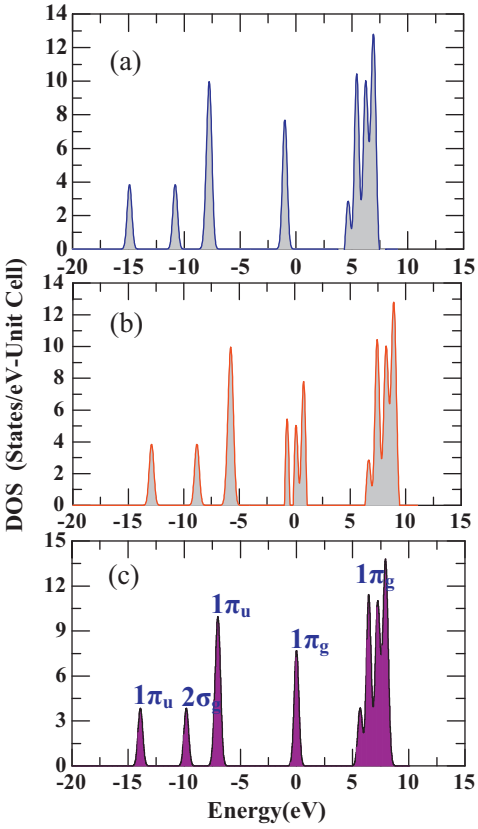

Fig. 11. PDOS of the adsorbed oxygen on (a) clean and (b) Nb doped TiO_2 surfaces. (c) PDOS of a free oxygen molecule.

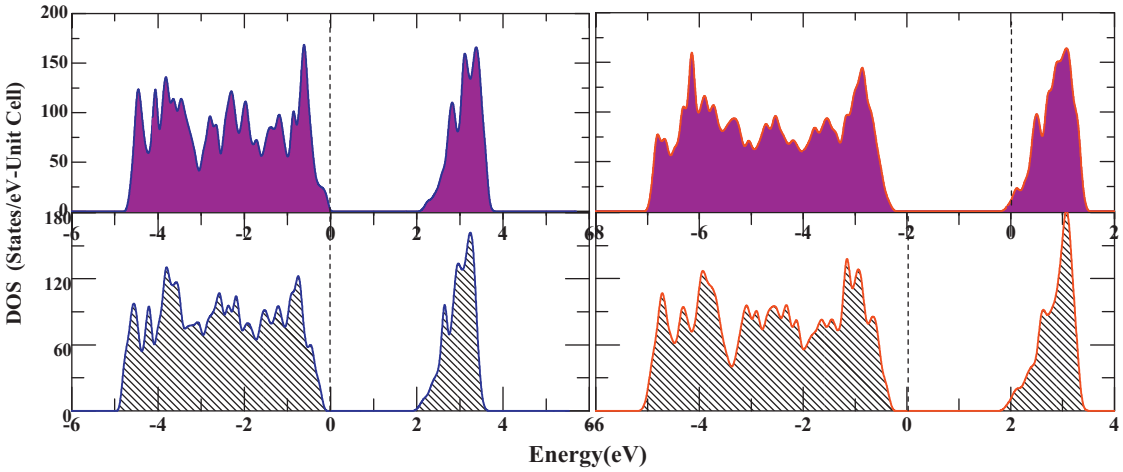

Fig. 12. PDOS of the (1 0 1) surface before and after oxygen adsorption for (a) clean (b) Nb doped TiO_2 surfaces.

Table 5
Oxygen adsorption energy for each model.

ΔE_{ads} (eV)	Ti_{5C} (Nb)	Ti_{6C}	O_{2C}	O_{3C}
TiO_2	−0.23	−0.18	0.12	0.04
TiO_2–Nb	−0.31 (0.26)	−0.22	0.08	0.02

formation energy, E_{form}, for each system was estimated using the relation [50]

$$E_{form}(\mathrm{Nb} \rightarrow \mathrm{Ti}) = E(\mathrm{Nb} \rightarrow \mathrm{Ti}) - E(\mathrm{TiO_2}) + \mu_{\mathrm{Ti}} - \mu_{\mathrm{Nb}} \quad (1)$$

where $E(TiO_2)$ and $E(\mathrm{Nb} \rightarrow \mathrm{Ti})$ are the energy of clean and doped surface, respectively, and μ_X (X = Ti, Nb) is atomic chemical potentials of X. Table 4 lists calculated E_{form}, where the substitution is lower in energy at the Ti_{5C} than the Ti_{6C} site, indicating that Nb prefers to occupy the Ti_{5C} site on the (1 0 1) surface.

As for the O adsorption, four candidate models are taken into account with the O adsorbed on Ti_{5C} (Nb in doped case), Ti_{6C}, O_{2C}, and O_{3C} sites, as illustrated in Fig. 10. To determine the most energetically favorable model, adsorption energy ΔE_{ads}, which is defined as reversible energy needed to separate an adsorption system into a clean surface (E_{surf}) and free oxygen (E_O), is calculated using the equation

$$\Delta E_{ads} = E_{ads} - E_{surf} - E_O \quad (2)$$

where E_{ads} is the energy of adsorption system. A negative ΔE_{ads} means that the process is exothermic and hence energetically stable. Table 5 summarizes our calculated ΔE_{ads} for both the clean and doped system, where the O is found to favor an adsorption on the Ti_{5C} site in comparison to other sites. Such adsorption energy is further lowered as Nb is added, having a value of −0.31 eV (−0.23 eV in clean case), indicating that the O–Ti_{5C} interaction turns stronger after doping, and that the doped surface promotes O adsorption.

Fig. 11 shows density of states (DOS) for the O adsorbed systems, where one can see that the O adsorbed on clean surface is similar in DOS to a free O, reflecting a minor change in electronic states of O. However, once Nb is added, DOS of adsorbed O is changed substantially: the $1\pi_g$ orbital becomes broadened, yet partially separated in an energy range of −1.0 to 1.0 eV, which implies a stronger interplay between the 2p orbitals of adsorbed O and 4d orbitals of Ti after doping. Fig. 12 shows DOS of surface atoms before and after O adsorption, where the change is minor *via* adsorption and the clean surface maintains a semiconducting nature. Interestingly, a donor-like state turns up near the bottom of conduction band in the doped case before adsorption, which is due to the extra electrons arising from Nb substitution. In addition, notable difference in DOS is seen after O adsorption: the E_F is shifted towards valence band, indicating that chemical interaction occurs between the adsorbed O and surface atoms.

Fig. 13 presents a charge distribution around E_F on each surface. A key feature is that the charge distribution alters dramatically *via* the Nb doping: charge is not seen in between adsorbed O and surface Ti_{5C} in clean case (Fig. 13(a)), yet visible in doped case (Fig. 13(b)). Further, the charges are accumulated between O and Ti in a spatially connected fashion (marked in Fig. 13(b)), which might serve as a conducting pathway, supporting the enhanced signal output observed in the doped case. To quantify charge transfer between adsorbed O and TiO_2, Table 6 lists Mullikan population of a typical O. The adsorbed O captures 0.06 *e* from the clean surface, whereas 0.32 *e* from the doped one, which indicates that the height of barrier is increased in the depletion layer after doping, and hence a higher gas response is likely once the VOC gas is in.

To provide firm evidence of the impact of adsorbed O on conductivity of TiO_2, we finally examine resistance of the sensor in air as a function of working temperature, as shown in Fig. 14. The resistance reduces gradually as the temperature is increased, which is attributed to the competitive processes between intrinsic electron

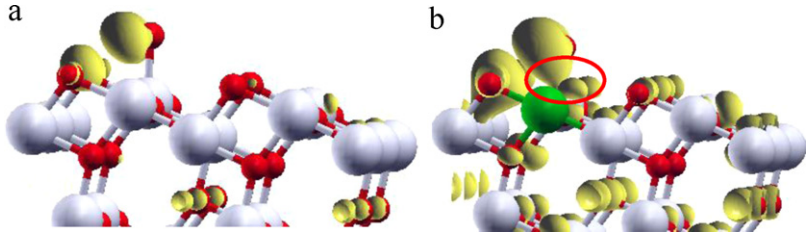

Fig. 13. Charge distribution around E_F for (a) clean (b) Nb doped TiO_2 surfaces.

Table 6
Mulliken charges for the free and adsorbed oxygen.

Before adsorption	2s	2p	Total
Free oxygen	1.82	4.12	5.94
After adsorption			
TiO_2 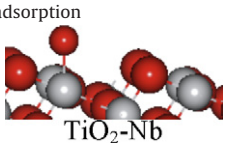	1.87	4.13	6.00
TiO_2–Nb 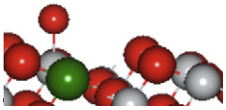	1.97	4.29	6.26

The inset figures present the site view of the surface model.

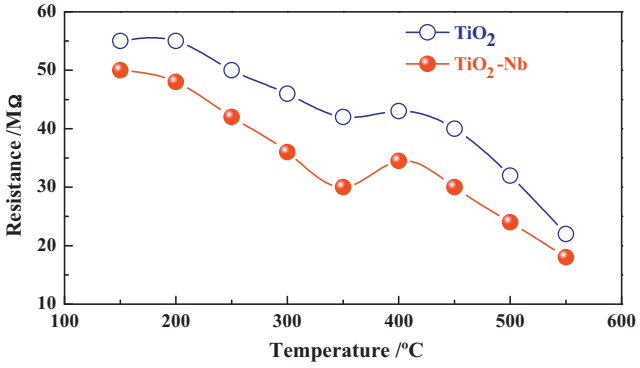

Fig. 14. Variation in the resistance of the TiO_2 sensors as a function of the operating temperature.

excitation and electron transfer from the oxide surface to adsorbed O that deteriorates electron transport across surface [51,52]. Interestingly, as the temperature is elevated from 350 to 400 °C, the resistance is increased only slightly, indicating that the absorbed O plays an important role. However, the resistance decreases as the temperature goes beyond 400 °C, suggesting that the intrinsic electron excitation dominates at high temperature. As compared to the pristine TiO_2, the doped one undergoes a larger extent of increase in resistance, which indicates that the doped surface is able to capture more amount of O. This, together with the remarkable difference in response to VOC gas between the pristine and doped TiO_2, reveals that more amount of O is pre-adsorbed on the doped surface, which ultimately results in an enhancement of gas-sensing response of TiO_2.

4. Conclusions

We have applied a simple yet efficient hydrothermal method to prepare pristine and Nb doped TiO_2 nano-composites, and investigated their microstructures and gas-sensing behavior to the VOC gases. The Nb doping is found to play an essential role in improving the gas response of anatase TiO_2 toward VOCs, the mechanism of which is clarified upon theoretical surface models. In comparison to the clean (1 0 1) surface, the doped one shows enhanced O adsorption and charge transfer, resulting in larger change in electronic structure of TiO_2 and more pronounced response to VOCs. Such findings may open up a new feasible way for understanding sensing mechanism of the TiO_2-based gas-sensing materials.

Acknowledgements

This work was supported in part by the Fundamental Research Funds for the Central University (CDJXS10131154) and the distinguished PhD foundation from the Ministry of Education of China (0903005109044-13).

References

[1] X. Wang, Y. Zhang, J. Xiong, Correlation between the solid/air partition coefficient and liquid molar volume for VOCs in building materials, Atmos. Environ. 42 (2008) 7768–7774.
[2] K.P. Chao, S.K. Ong, M. Huang, Mass transfer of VOCs in laboratory-scale air sparging tank, J. Hazard. Mater. 152 (2008) 1098–1107.
[3] W.B. Li, J.X. Wang, H. Gong, Catalytic combustion of VOCs on non-noble metal catalysts, Catal. Today 148 (2009) 81–87.
[4] A.K. Srivastava, Vinayak P. Dravid, On the performance evaluation of hybrid and mono-class sensor arrays in selective detection of VOCs: a comparative study, Sensors Actuat. B 117 (2006) 244–252.
[5] V.C. Gonçalves, D.T. Balogh, Optical VOCs detection using poly (3-alkylthiophenes) with different side-chain lengths, Sensors Actuat. B 142 (2009) 55–60.
[6] M. Mori, H. Nishimura, Y. Itagaki, Y. Sadaoka, E. Traversa, Detection of sub-ppm level of VOCs based on a Pt/YSZ/Pt potentiometric oxygen sensor with reference air, Sensors Actuat. B 143 (2009) 56–61.
[7] M. Consales, S. Campopiano, A. Cutolo, M. Penza, P. Aversa, G. Cassano, M. Giordano, A. Cusano, Carbon nanotubes thin films fiber optic and acoustic VOCs sensors: performances analysis, Sensors Actuat. B 118 (2006) 232–242.
[8] M. Penza, G. Cassano, P. Aversa, F. Antolini, A. Cusano, M. Consales, M. Giordano, L. Nicolais, Carbon nanotubes-coated multi-transducing sensors for VOCs detection, Sensors Actuat. B 111–112 (2005) 171–180.
[9] W. Zeng, T. Liu, Z. Wang, Enhanced gas sensing properties by SnO_2 nanosphere functionalized TiO_2 nanobelts, J. Mater. Chem. 22 (2012) 3544–3548.
[10] A.K. Srivastava, Detection of volatile organic compounds (VOCs) using SnO_2 gas-sensor array and artificial neural network, Sensors Actuat. B 96 (2003) 24–37.
[11] W.M. Zhang, J.S. Hu, W.G. Song, L.J. Wan, Detection of VOCs and their concentrations by a single SnO_2 sensor using kinetic information, Sensors Actuat. B 123 (2007) 454–460.
[12] W. Zeng, T. Liu, Z. Wang, S. Tsukimoto, M. Saito, Y. Ikuhara, Selective detection of formaldehyde gas using a Cd-doped TiO_2–SnO_2 sensor, Sensors 9 (2009) 9029–9038.
[13] B.L. Zhu, C.S. Xie, W.Y. Wang, K.J. Huang, J.H. Hu, Improvement in gas sensitivity of ZnO thick film to volatile organic compounds (VOCs) by adding TiO_2, Mater. Lett. 28 (2004) 624–629.
[14] W. Zeng, T. Liu, Gas-sensing properties of SnO_2–TiO_2-based sensor for volatile organic compound gas and its sensing mechanism, Physica B 405 (2010) 1345–1348.
[15] D.S. Lee, J.K. Jung, J.W. Lim, J.S. Huh, D.D. Lee, Recognition of volatile organic compounds using SnO_2 sensor array and pattern recognition analysis, Sensors Actuat. B 77 (2001) 228–236.
[16] Y. Gui, S. Li, J. Xu, C. Li, Study on TiO_2-doped ZnO thick film gas sensors enhanced by UV light at room temperature, Microelectron. J. 39 (2008) 1120–1125.
[17] A. Teleki, S.E. Pratsinis, K. Kalyanasundaram, P.I. Gouma, Sensing of organic vapors by flame-made TiO_2 nanoparticles, Sensors Actuat. B 119 (2006) 683–690.
[18] N.E. Stankova, I.G. Dimitrov, T.R. Stoyanchov, P.A. Atanasov, Optical and gas sensing properties of thick TiO_2 films grown by laser deposition, Appl. Surf. Sci. 254 (2007) 1268–1272.
[19] W. Moon, K. Lee, Y. Jun, H. Kim, S. Hong, Orientation dependence of gas sensing properties of TiO_2 films, Sensors Actuat. B 115 (2006) 123–127.
[20] I. Hayakawa, Y. Iwamoto, K. Kikuta, S. Hirano, Gas sensing properties of platinum dispersed-TiO_2 thin film derived from precursor, Sensors Actuat. B 62 (2000) 55–60.
[21] W. Zeng, T.M. Liu, D.J. Liu, C.L. Lv, Hydrothermal synthesis and volatile organic compounds sensing properties of La–TiO_2 nanobelts, Physica E 44 (2011) 37–42.
[22] Y.C. Wu, X.Y. Hu, T. Xie, G.H. Li, L.D. Zhang, Phase structure of W-doped nano-TiO_2 produced by sol–gel method, China Particuol. 3 (2005) 233–236.
[23] M. Ferroni, M.C. Carotta, V. Guidi, G. Martinelli, F. Ronconi, O. Richard, D. Van Dyck, J. Van Landuyt, Structural characterization of Nb–TiO_2 nanosized thick-films for gas sensing application, Sensors Actuat. B 48 (2000) 140–145.
[24] M.C. Carotta, M. Ferroni, D. Gnani, V. Guidi, M. Merli, G. Martinelli, M.C. Casale, M. Notaro, Nanostructured pure and Nb-doped TiO_2 as thick film gas sensors for environmental monitoring, Sensors Actuat. B 58 (1999) 310–317.
[25] J.A. Park, J.H. Moon, S.J. Lee, S.H. Kim, T.H. Zyung, H.Y. Chu, Structural, electrical and gas sensing properties of eletrospun TiO_2 nanofibers, Thin Solid Films 518 (2010) 6642–6645.
[26] M. Kudo, T. Kosaka, Y. Takahashi, H. Kokusen, N. Sotani, S. Hasegawa, Sensing functions to NO and O_2 of Nb_2O_5- or Ta_2O_5-loaded TiO_2 and ZnO, Sensors Actuat. B 69 (2000) 10–15.
[27] A.M. Ruiz, G. Dezanneau, J. Arbiol, A. Cornet, J.R. Morante, Insights into the structural and chemical modifications of Nb additive on TiO_2 nanoparticles, Chem. Mater. 16 (2004) 862–871.

[28] T. Nikolay, L. Larina, O. Shevaleevskiy, B.T. Ahn, Electronic structure study of lightly Nb-doped TiO_2 electrode for dye-sensitized solar cells, Energy Environ. Sci. 4 (2011) 1480–1486.
[29] Y. Gao, S. Thevuthasan, D.E. McCready, M. Engelhard, MOCVD growth and structure of Nb- and V-doped TiO_2 films on sapphire, J. Cryst. Growth 212 (2000) 178–190.
[30] T. Anukunprasert, C. Saiwan, E. Traversa, The development of gas sensor for carbon monoxide monitoring using nanostructure of Nb–TiO_2, Sci. Technol. Adv. Mater. 6 (2005) 359–363.
[31] A. Teleki, N. Bjelobrk, S.E. Pratsinis, Flame-made Nb and Cu doped TiO_2 sensors for CO and ethanol, Sensors Actuat. B 130 (2008) 449–457.
[32] E. Comini, G. Faglia, G. Sberveglieri, Y.X. Li, W. Wlodarski, M.K. Ghantasala, Sensitivity enhancement towards ethanol and methanol of TiO_2 films doped with Pt and Nb, Sensors Actuat. B 64 (2000) 169–174.
[33] M.G. Manera, P.D. Cozzoli, G. Leo, M.L. Curri, A. Agostiano, L. Vasanelli, R. Rella, Thin films of TiO_2 nanocrystals with controlled shape and surface coating for surface plasmon resonance alcohol vapour sensing, Sensors Actuat. B 126 (2007) 562–572.
[34] W. Zeng, T. Liu, Z. Wang, Sensitivity improvement of TiO_2-doped SnO_2 to volatile organic compounds, Physica E 43 (2010) 633–638.
[35] M.H. Seo, M. Yuasa, T. Kida, J.S. Huh, K. Shimanoe, N. Yamazoe, Gas sensing characteristics and porosity control of nanostructured films composed of TiO_2 nanotubes, Sensors Actuat. B 137 (2009) 513–520.
[36] E. Comini, M. Ferroni, V. Guidi, A. Vomiero, P.G. Merli, V. Morandi, M. Sacerdoti, G. Della Mea, G. Sberveglieri, Effects of Ta/Nb-doping on titania-based thin films for gas-sensing, Sensors Actuat. B 108 (2005) 21–28.
[37] D.E. Williams, Semiconducting oxides as gas-sensitive resistors, Sensors Actuat. B 57 (1999) 1–16.
[38] G. Korotcenkov, Gas response control through structural and chemical modifications of metal oxide films: state of the art and approaches, Sensors Actuat. B (2005) 209–232.
[39] A. Vittadni, M. Casarin, A. Selloni, Chemistry of and on TiO_2-anatase surfaces by DFT calculations: a partial review, Theor. Chem. Acc. 117 (2007) 663–671.
[40] A. Selloni, A. Vittadini, M. Grätzel, The adsorption of small molecules on the TiO_2 anatase (1 0 1) surface by first-principles molecular dynamics, Surf. Sci. 402–404 (1998) 219–222.
[41] A.V. Bandura, R.A. Evarestov, From anatase (1 0 1) surface to TiO_2 nanotubes: rolling procedure and first principles LCAO calculations, Surf. Sci. 603 (2009) 117–120.
[42] A. Vittadini, A. Selloni, A. Rotzinger, Structure and energetic of water adsorbed at TiO_2 anatase (1 0 1) and (0 0 1) surfaces, Phys. Rev. Lett. 81 (1998) 2955–2957.
[43] Q. Chen, C. Tang, G. Zheng, First-principles study of TiO_2 anatase (1 0 1) surfaces doped with N, Physica B 404 (2009) 1074–1078.
[44] M. Nilsing, S. Lunell, P. Persson, L. Ojamäe, Phosphonic acid adsorption at the TiO_2 anatase (1 0 1) surface investigated by periodic hybrid HF-DFT computations, Surf. Sci. 582 (2005) 49–60.
[45] W. Zeng, T. Liu, Z. Wang, S. Tsukimoto, M. Saito, Y. Ikuhara, Oxygen adsorption on anatase TiO_2 (1 0 1) and (0 0 1) surfaces, Mater. Trans. 51 (2010) 171–175.
[46] J.K. Burdett, T. Hughbanks, G.J. Miller, J.W. Richardson Jr., J.V. Smith, Structural–electronic relationships in inorganic solids: powder neutron diffraction studies of the rutile and anatase polymorphs of titanium dioxide at 15 and 295 K, J. Am. Chem. Soc. 109 (1987) 3639–3646.
[47] J.C. Slater, The electronic structure of atoms – the Hartree–Fock method and correlation, Rev. Mod. Phys. 35 (1963) 484–487.
[48] P. Perdew, Y. Wang, Accurate and simple density functional for the electronic exchange energy: generalized gradient approximation, Phys. Rev. B 33 (1986) 8800–8802.
[49] U. Diebold, The surface science of titanium dioxide, Surf. Sci. Rep. 48 (2003) 53–229.
[50] W. Zeng, T.M. Liu, C.L. Lv, D.J. Liu, Atomic and electronic structures of Mg-doped perfect $SrTiO_3$ and crystals containing oxygen vacancies from first principles, Physica B 406 (2011) 1420–1428.
[51] M. Egshira, Y. Shimizu, Y. Takao, S. Sako, Variations in I–V characteristics of oxide semiconductors induced by oxidizing gases, Sensors Actuat. B 35 (1996) 62–67.
[52] M. Che, A.J. Tench, Characterization and reactivity of molecular oxygen species on oxide surfaces, Adv. Catal. 32 (1983) 1–148.

Biographies

Wen Zeng received his PhD degree in material science from Chongqing University in China in 2010. He was a visiting scholar at Tohoku University in Japan from 2009 to 2010. He is currently a lecture at the College of Materials Science and Engineering, Chongqing University. His current research includes the synthesis of low-dimensional functional materials, the fabrication of semiconductor sensor, and the first principles calculations.

Tianmo Liu is a professor of College of Materials Science and Engineering at Chongqing University in China since 2001. He received Dr. Eng. from Department of Solid Mechanics, Chongqing Univ. in 1999. His current research interest involves functional gas-sensing materials, magnesium alloys, and theoretical calculations. He is now also holding a group leader position at National Engineering Research Center for Magnesium Alloys at Chongqing University.

Zhongchang Wang is now an assistant professor at the world premier international research center, advanced institute for materials research, Tohoku University in Japan. He received his PhD in 2007 from The University of Tokyo in Japan. He is currently mainly focusing on gas-sensing materials, interfaces, grain boundaries, dislocations in functional oxides, and quantum transport *via* combining the advanced transmission electron microscopy with the first-principles calculations.